Noise masking of S-cone increments and decrements

Quanhong Wang*
Psychology Department, Northeastern University, Boston, MA, USA

David P. Richters
Psychology Department, Northeastern University, Boston, MA, USA

Rhea T. Eskew Jr.
Psychology Department, Northeastern University, Boston, MA, USA

S-cone increment and decrement detection thresholds were measured in the presence of bipolar, dynamic noise masks. Noise chromaticities were the L-, M-, and S-cone directions, as well as L–M, L+M, and achromatic (L+M+S) directions. Noise contrast power was varied to measure threshold Energy versus Noise (EvN) functions. S+ and S– thresholds were similarly, and weakly, raised by achromatic noise. However, S+ thresholds were much more elevated by S, L+M, L–M, L- and M-cone noises than were S– thresholds, even though the noises consisted of two symmetric chromatic polarities of equal contrast power. A linear cone combination model accounts for the overall pattern of masking of a single test polarity well. L and M cones have opposite signs in their effects upon raising S+ and S– thresholds. The results strongly indicate that the psychophysical mechanisms responsible for S+ and S– detection, presumably based on S-ON and S-OFF pathways, are distinct, unipolar mechanisms, and that they have different spatiotemporal sampling characteristics, or contrast gains, or both.

Introduction

In the retina-geniculate-striate system there are separate pathways that carry excitatory responses to cone increment and decrement signals, the ON and OFF pathways (Kuffler, 1953; Schiller, 1992). Recent attention has focused on ON and OFF pathways that carry signals generated by short-wavelength-sensitive (S) cones, which are anatomically and physiologically distinct from one another (see the recent review by Dacey, Crook, & Packer, 2014).

In the ON pathway, S-cone signals are passed to S-cone ON bipolars (Kouyama & Marshak, 1992; Mariani, 1984), and from there, to at least two ganglion cell types, the small and large bistratified cells (Dacey, 1996; Dacey & Lee, 1994; Dacey, Peterson, Robinson, & Gamlin, 2003). In contrast, S-OFF signals in the central retina may be initially carried by a midget bipolar cell (Klug, Herr, Ngo, Sterling, & Schein, 2003; Klug, Tsukamoto, Sterling, & Schein, 1993); at the ganglion cell level, a large monostratified cell receiving inhibitory input from S cones has been identified (Dacey & Packer, 2003). Other, less well-studied anatomical connections exist for both S-ON and S-OFF signals (Dacey et al., 2014). Anatomical differences persist in the cortex: S-ON and S-OFF pathways are anatomically segregated at the level of V1 (Chatterjee & Callaway, 2003).

Given these anatomical distinctions it is unsurprising that physiological differences between these two pathways have been reported. At the level of the lateral geniculate nucleus (LGN), S-ON receptive fields are smaller (Tailby, Solomon, & Lennie, 2008) and more bandpass than S-OFF receptive fields at similar eccentricities (Tailby, Szmajda, Buzas, Lee, & Martin, 2008). S-ON cells have been found to be more responsive to S-cone modulations (Tailby, Solomon, & Lennie, 2008; Tailby, Szmajda et al., 2008), and show more saturation in their contrast response curves than S-OFF cells (Solomon & Lennie, 2005; Tailby, Solomon, & Lennie, 2008). More contrast gain control has been found in S-ON than S-OFF LGN, but not cortical, cells (Solomon & Lennie, 2005).

Although there are L-ON, L-OFF, M-ON, and M-OFF cells, little asymmetry in L- or M-cone increment and decrement detection has been reported; psychophysically, under many conditions, thresholds of L- and M-cone isolating stimuli are mediated by symmetric, postreceptoral mechanisms that receive opposite and approximately equal L- and M-cone contrast inputs, the R (L–M) and G (M–L) mechanisms

Citation: Wang, Q., Richters, D. P., & Eskew, R. T. (2014). Noise masking of S-cone increments and decrements. *Journal of Vision, 14*(13):8, 1–17. http://www.journalofvision.org/content/14/13/8, doi: 10.1167/14.13.8.

doi: 10.1167/14.13.8 Received May 30, 2014; published November 12, 2014 ISSN 1534-7362

(Chaparro, Stromeyer, Chen, & Kronauer, 1995; Eskew, McLellan, & Giulianini, 1999; Stromeyer, Cole, & Kronauer, 1985; Vingrys & Mahon, 1998). In contrast, a number of psychophysical studies have found evidence for qualitative as well as quantitative differences between detection and discrimination of S-cone increment and decrement stimuli, differences that suggest functional distinctions between these two pathways. These increment/decrement findings include differences in the long-wavelength signals opposing S-cone signals (McLellan & Eskew, 2000); different patterns of threshold elevations following background modulations (Krauskopf, Williams, Mandler, & Brown, 1986; Shapiro & Zaidi, 1992; Shinomori, Spillmann, & Werner, 1999); differences in pedestal masking (Gabree & Eskew, 2006; Vingrys & Mahon, 1998); differences in temporal impulse response functions (Shinomori & Werner, 2008); and differences in spatial integration (Vassilev, Mihaylova, Racheva, Zlatkova, & Anderson, 2003; Vassilev, Zlatkova, Manahilov, Krumov, & Schaumberger, 2000) and acuity (Zlatkova, Vassilev, & Anderson, 2008). Smithson (2014) has recently reviewed these differences.

The present experiment uses noise masks to raise S-cone increment and decrement thresholds. Bipolar noises, containing two complementary chromaticities so that the mean chromaticity and luminance is constant, were varied in their contrast, and the effects on S+ and S– tests measured. Noise color directions were the L-, M-, and S-cone directions; and mixtures L–M, L+M, and L+M+S (achromatic). Data from these energy versus noise (EvN) measurements were then combined across noise chromaticities, and a linear chromatic detection mechanism model fit to the entire data set to derive cone weights for S+ and S– tests separately. The results show that the identical masking noise has a much greater effect on S+ tests than S– ones. Given previous results indicating nonlinearities in S-cone detection (Giulianini & Eskew, 2007; McLellan & Eskew, 2000), a linear cone combination model provides a surprisingly good fit to the data, with the L and M cone weights being of opposite sign.

Methods

Observers

Two observers (QW and DR) were used in the main study, and one additional one (RTE) in the rod control conditions. Total error scores on the Farnsworth-Munsell 100 Hue Test (FM-100) were low and showed no error axis for the three observers. QW and RTE were corrected to normal acuity using spectacle lenses or trial lenses (DR is emmetropic). Two (DR and RTE) were highly-experienced psychophysical observers at the start of the study. The other observer, QW, was less experienced, and showed evidence of a long-term practice effect that particularly reduced the S+ thresholds. A similar long-term practice effect was reported by Giulianini and Eskew (2007). The data shown in this paper were collected after more than a month of practice by QW, and showed no evidence of further reductions in threshold. The research protocol was approved by Northeastern University's Institutional Review Board; the procedures comply with the Declaration of Helsinki.

Apparatus and calibration

Stimuli were created on a Macintosh computer and displayed on a Sony Trinitron monitor running at a 75-Hz frame rate by a video board with 10-bit digital-to-analog converters. The mean field provided by the monitor was white ($x = 0.301$, $y = 0.313$), with a luminance of 50.2 cd/m^2. Viewing was monocular using the natural pupil, with head position stabilized by a chin rest. The viewed area was 24.0° wide and 21.2° high. Fixation was guided by four black diagonal lines pointed at the center of the screen, ending 1.27° from the center.

An Ocean Optics spectroradiometer (Ocean Optics, Dunedin, FL) was used to calibrate the three guns of the monitor at 1 nm intervals across the visible spectrum. These spectral calibrations were also checked with a Photo Research PR650 spectroradiometer (PhotoResearch, Chatsworth, CA). Gamma correction of the monitor output was achieved via software lookup tables.

S-cone isolation

S-cone isolating stimuli were produced by changes in the monitor guns that were calculated to be silent substitutions for both L and M cones: they caused either increments or decrements in S-cone quantal catch without altering the quantal catch rates of the other two cone classes. The short-wavelength cone isolating direction for a standard observer in the color space of our monitor primaries was determined by cross-multiplying the monitor gun spectra with the Stockman and Sharpe (2000) 2-deg cone fundamentals, interpolated to 1 nm intervals. The validity of this isolating direction was examined for two observers (DR and RTE) by use of the following method (McLellan & Eskew, 2000; Webster & Mollon, 1994). Observers viewed the monitor through a beamsplitter cube mounted close to the eye. A circular field of violet, 420 nm light of ca. 17 td (as seen through the beamsplitter),

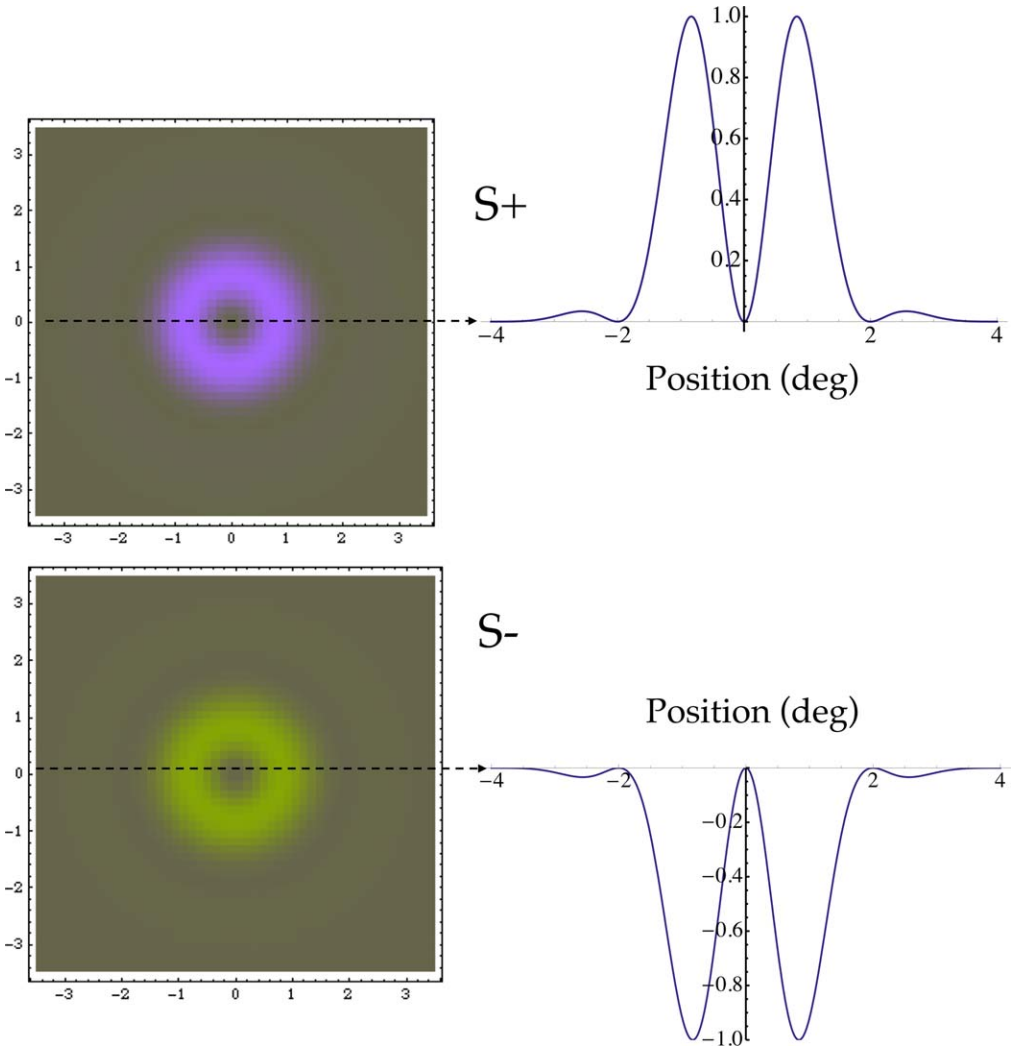

Figure 1. Test stimuli. These are radial raised Gabors, with peak contrasts near 1° eccentricity. A depiction of the stimuli is shown on the left, and their contrast profiles are at the right.

from a separate optical channel, was combined in the beamsplitter with the monitor image, covering the central region of the monitor image. This weak violet field provides approximately four-fold greater dilution of the S-cone contrast than that of the L or M cones, and thereby raises S-cone mediated thresholds more than those mediated by the other cone classes.

The observers used the method of adjustment to measure detection thresholds, through the beamsplitter, with and without the 420 nm added field. The nominal S-cone isolating direction based upon the Stockman and Sharpe fundamentals, and nearby directions in RGB space, were used. For both observers, the Stockman and Sharpe isolating direction was maximally elevated by the blue added field, and thus was taken to be the actual S-cone isolating direction. For QW, whose results were qualitatively very similar to DR and RTE, the Stockman and Sharpe direction was assumed.

Tests and noise

Figure 1 depicts the S+ and S– tests, along with their contrast profiles. The test was presented as a rectangular flash of 200 ms duration. The spatial profile of the test stimulus was designed to favor detection by S cones, to guard against any failures of cone isolation. The test was annular, with a contrast peak about 1° outside the central fovea near where S-cone density is highest, and no contrast in central fovea where S cones are absent (Curcio et al., 1991; Williams, MacLeod, & Hayhoe, 1981). Its spatial contrast profile is a radial, raised Gabor function of eccentricity ρ (in degrees of visual angle), $ke^{-\frac{\rho^2}{2\sigma^2}}[1 - Cos(2\pi f\rho)]$, with the normalizing constant $k = 0.7584$ for $f = 1/2$ cpd and $\sigma = 1°$.

The binary masking noise, samples of which are depicted in the top section of Figure 2, consisted of rings that filled the screen, and flickered continuously through the experimental run. The rings were two

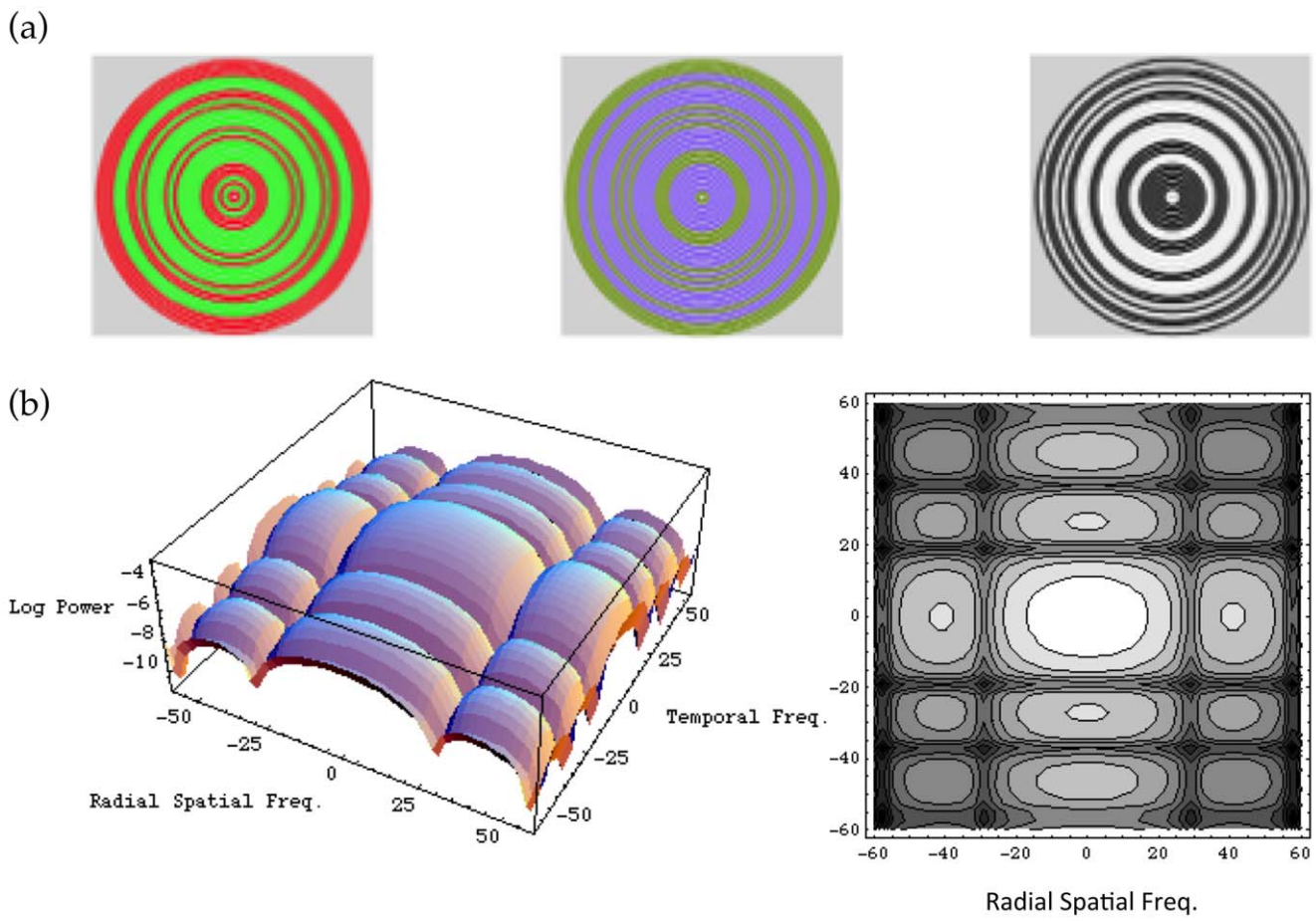

Figure 2. Masking noise. Noise rings were binary, randomly switching between two complimentary chromaticities with probability 1/2 at 18.75 Hz. The three panels in (a) depict three examples of the noise, for L–M, S, and achromatic chromaticities. The panels in (b) show the power spectrum of the masking noise, in terms of temporal and (radial) spatial frequency, as a surface plot and a contour plot. See Appendix A.

pixels wide, and separated by a gap of two pixels in which the test appeared (Giulianini & Eskew, 1998); between test presentations, the two-pixel gap was set to the mean field. The "half-toning" was also used in no-noise conditions: the rings were drawn with zero contrast and modulated as if they were present, to be certain that no artifacts in software could alter the timing of the stimulus presentation. We used three noise power magnitudes at each noise chromaticity: a value near the maximum permitted by the apparatus, half that value, and zero. For S-cone noise, additional noise levels were used (see Figure 3).

The rings randomly and independently changed from one chromaticity to a symmetrically opposite chromaticity (on the opposite side of the white point), so that the mean chromaticity was unchanged. Each ring switched chromaticity with probability 1/2 at 18.75 Hz. Samples of the noise are binomially distributed; when the visual system integrates the noise over space and time, the resulting sampling distribution will be approximately Gaussian for sufficiently large samples (note, however, that it is not necessary to assume a Gaussian distribution of noise effects here). The bottom panels of Figure 2 plot the power spectrum of the noise, which is derived in Appendix A. The plot shows that the noise has power over a broad range of frequencies; because there is substantial power at low spatial and temporal frequencies, the noise readily masks the spatially-localized and flashed test, which is of course also dominated by low frequencies. The value of the noise power spectrum at DC is taken as the proportionality between squared contrast and noise power. Units of test contrast energy are also derived in Appendix A.

Noise along the L, M, S, L–M (equal and opposite contrasts in L and M), L+M (equal contrasts in L and M), and achromatic (equal contrasts in L, M, and S) directions were used. L+M, the luminance *mechanism* direction, is the chromaticity that most efficiently stimulates the luminance mechanism in the cardinal axis model (Krauskopf, Williams, & Heeley, 1982), whereas the achromatic, L+M+S direction is the

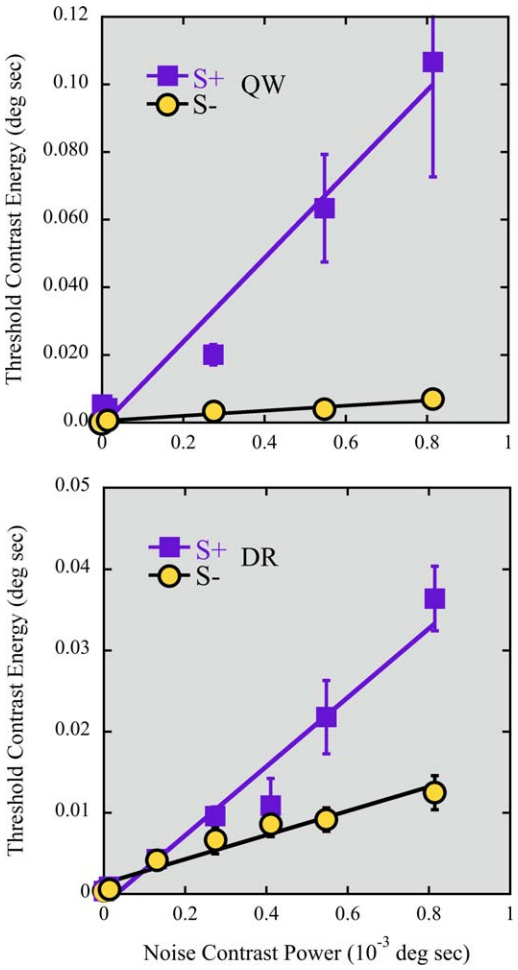

Figure 3. EvN functions for S+ (squares) and S– (circles) tests in S cone noise, for two observers (on different vertical scales). The S+ function is ~3 (DR) to 16 (QW) times steeper than the S– function, even though the noise contains equal amounts of incremental and decremental S-cone contrast. Standard error bars are shown where they are larger than the symbols.

luminance *isolating* direction, the chromaticity that does not stimulate any other mechanism (Eskew et al., 1999). With the exception of Table 1, stimulus strengths are reported in squared units: cone contrast energy or power (Appendix A).

Procedure

Detection thresholds were measured with a forced choice, two temporal alternative, adaptive staircase procedure. Observers adapted to the white background field for 2 min before each run of 100 trials. In noise conditions the observer adapted to the background plus the flickering masking noise. Each trial consisted of two 200 ms intervals signaled by beeps and separated by 400 ms. The observer initiated each trial, pressed a button to indicate the test interval, and received feedback after the response. Test contrast was decreased by 0.1 log units after three consecutive correct responses and increased by the same amount after one incorrect response. Two independent staircases were randomly interwoven within a run. Weibull functions were fit to the accumulated frequency-of-seeing data from a run using a maximum likelihood method (Pelli & Zhang, 1991; Watson, 1979) to estimate two parameters of the psychometric function for the test: a threshold estimate corresponding to detection rate of 82% and an estimate of the psychometric slope.

Two to four runs were obtained for most noise powers, with runs occurring in different sessions on different days; for QW, in three of the 40 cases, only one run was available at a particular noise power. In any given session, the test polarity was either S+ or S–. Observer DR intermixed different noise directions (and the no-noise condition) across all sessions, whereas for QW the noise directions were blocked. Consequently, in the analysis of QW's EvNs the no-noise thresholds were taken from each block, whereas for DR a single no-noise threshold was used for all the EvNs for each test polarity.

	DR	QW
S+	0.026 (0.001)	0.067 (0.008)
S–	0.023 (0.001)	0.053 (0.007)
S+/S–	1.14	1.21

Table 1. Mean no-noise S-cone thresholds and (standard errors). Cone contrast (not energy) units.

Results and discussion

Unmasked S+ versus S–

The mean no-noise thresholds for DR and QW, in cone contrast (not energy) units, are shown in Table 1. Several previous reports (Giulianini & Eskew, 2007; McLellan & Eskew, 2000; Vassilev et al., 2003) indicate that unmasked near-foveal S+ thresholds are higher than S– thresholds, at least for some observers, and our results are consistent with those reports, but without masking noise these differences are small and not statistically significant (cf. Bosten et al., 2014).

Masked S+ versus S–

All the chromatic noises (L, M, S, L+M, and L–M) produced substantial masking and substantial differences between S+ and S–. S-cone noise EvNs for two observers are shown in Figure 3. Squares represent the increment EvN, and circles represent the decrement

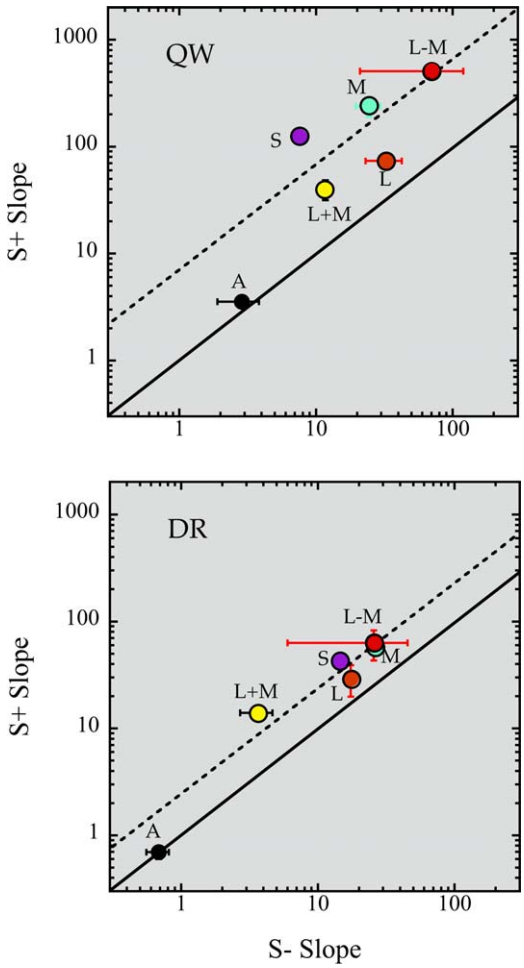

Figure 4. Slope comparison of S+ and S– EvNs, on log-log coordinates, for two observers. The solid line shows equality of slopes. The dashed line shows the mean log difference (excluding the achromatic, L+M+S, slopes). Vertical and horizontal standard error bars are drawn when larger than the symbols. For both observers, the difference between S+ and S– slope is significantly greater than zero (paired t tests, $p < 0.05$), whether or not the achromatic slopes are included.

EvN. As shown, both S+ and S– detection energies increase with S-cone noise power, but the S+ thresholds increase much faster.

These data indicate that test cone contrast energy is approximately linearly related to the noise cone contrast power, consistent with a large body of prior research with both achromatic and chromatic stimuli (e.g., Gegenfurtner & Kiper, 1992; Giulianini & Eskew, 1998; Lu & Dosher, 2008; Pelli, 1990). This linear relationship between test cone contrast energy E_t and noise cone contrast power N may be represented as

$$E_t = N_0 + bN \quad (1)$$

with b being the slope. The intercept, N_0, must be the same for a given test (S+ or S–) across all noise chromaticities, within measurement error, so it is the slope, which represents the (field) sensitivity to the noise chromaticity, that is of most interest here.

The lines in Figure 3 show the fit of Equation 1 to the S-cone EvNs. The higher no-noise thresholds for S+, as shown in Table 1, mean that the vertical intercept N_0 values of the EvN (the estimate of intrinsic noise), which is proportional to the squared no-noise thresholds (Appendix A), are slightly greater for S+ than S–.

For DR, the slope b (with 95% confidence intervals) of the EvN for is 42.5 (±10.3) for increment and 14.8 (±4.1) for decrement tests; the corresponding slopes are 123.9 (±43.4) and 7.5 (±2.6) for QW. The difference in the slopes indicates a robust asymmetry in the masking effects on S increment and decrement detections produced by the S-cone noise, which itself contains equal amounts of increment and decrement contrast and is identical for the two test polarities. There is a suggestion of a deceleration in the S– EvN for both observers (and, to a lesser degree, an acceleration in the S+ function).

S+ and S– EvNs were also measured with L+M+S (achromatic), L, M, L+M, and L–M noises, with three noise power levels for each function. None of these EvNs showed any strong suggestion of nonlinearity, although with only three levels of power this is not in any way conclusive. Slopes of the fits of Equation 1 for all of these cases are shown in Figure 4, which plots the fitted b values for the two tests against one another on log-log coordinates. The solid line indicates equality of slopes for the two test polarities. The achromatic slopes lie near that line, for both observers: achromatic, L+M+S noise has approximately the same effect on S+ and S– tests (slope ratio of 1.2 and 1.0 for QW and DR, respectively). The chromatic slopes all fall above that line, showing that the same noise has a greater effect on S+ tests; these EvNs are also much steeper than the achromatic EvNs.

Thus, S+ detection is much more masked than S– detection, by identical noises, across a wide range of noise chromaticities. The only exception is achromatic, L+M+S noise.

The dashed line shows a constant log difference of 2.6-fold (DR) and 7.8-fold (QW), the mean ratio for each observer (excluding the achromatic slopes). For DR, the chromatic noise S+/S– difference is well characterized as being a constant factor, as if there were a difference in masking efficiency between the two mechanisms. For QW, the pattern is noisier but is roughly consistent with DR.

Chromatic masking may be understood with reference to the *mechanism noise* or the noise as seen by a hypothetical chromatic mechanism (Giulianini & Eskew, 2007). As discussed in Appendix C, the relationship between test energy E_t and the mechanism noise is an elaboration of Equation 1:

Test polarity	Observer	Vector length	W_l	W_m	W_s	r^2
S+	DR	10.05	0.31 (0.28)	−0.74 (0.29)	0.59 (0.03)	0.94
	QW	21.95	0.39 (0.10)	−0.77 (0.10)	0.50 (0.01)	0.98
S−	DR	6.18	0.32 (0.41)	−0.73 (0.42)	0.60 (0.05)	0.89
	QW	6.64	0.18 (0.21)	−0.94 (0.22)	0.30 (0.03)	0.97

Table 2. Noise effectiveness (vector length), relative cone contrast weights (*W*s) and (their standard errors), and goodness of fit (r^2) of Equation 3. Note that the overall sign of the three weights in each row is unknown (see text). Equation 9, Appendix C, gives the interpretation of the vector length.

$$E_t = N_0 + aQ_n f^2(l_n, m_n, s_n). \quad (2)$$

with l_n, m_n, and s_n representing the cone contrast components of the noise, $f()$ the combination of these cone contrasts, Q_n a constant representing the spatiotemporal characteristics of the noise (Appendix A), a representing the sensitivity of the mechanism to the noise's spatiotemporal characteristics, and N_0 the no-noise test energy. If the cone combination is linear, f is a weighted sum of the three cone contrasts and we may rewrite Equation 2 as

$$E_t = N_0 + aQ_n(W_l l_n + W_m m_n + W_s s_n)^2, \quad (3)$$

with the subscripted W_s being the cone contrast weights. This last equation was fit to each observer's energy thresholds (for 20 and 17 different cone contrast triplets for each test polarity for QW and DR, respectively), using a nonlinear least-squares method, to estimate values for the three weights. This procedure finds the best parabolic hypersurface to describe the relationship between threshold contrast energy elevation and the three cone contrast components of the noise.

Results are summarized in Table 2. The cone weights have been normalized such that they form a vector of unit length, with the vector length factored out; this magnitude incorporates the (unknown) value of a (see Appendix C). Because the cone combination is squared, the overall sign of the vector of weights is unknown; in each row of the table, the three cone weights could be reversed in sign without effect. Thus, we cannot determine, using this method, whether the S+ and S− weight vectors are of opposite sign.

The relative cone weights are remarkably consistent across test polarities and observer: they are nearly identical in three of the four cases (although, due to the somewhat limited sample size, a few of the standard errors are large). The S+ and S− vector lengths reflect the greater amount of masking for the S+ tests. The relative weights suggest that there is no spectral difference between S+ and S− masking. These weights show a very strong cone opponent, L–M, factor in the masking of S-cone tests by noise, consistent with the direct EvN measurements (Figure 4).

Figure 5 plots Equation 3 using the parameter values from Table 2, for the two observers in panels (a) and (b). In each panel, the middle pairs of figures show that the L and S weights are of the same sign: the thresholds are raised most near the same-signed, (−1,−1) and (1,1) corners. The top and bottom figures, in contrast, demonstrate that L and M, as well as M and S, are of opposite sign, with thresholds highest near the oppositely-signed, (−1,1) and (1,−1), corners. The greater masking of S+ is shown by the steeper rises in the surfaces in the left columns compared to the right columns over the same range of cone contrasts. Similarly, the greater masking shown by QW is demonstrated by the steeper rises of most of the surfaces in (a) compared to (b); an exception is the SL plane, middle panel, where the relatively small L- and S-cone weights make this surface look relatively flat on this scale. The lack of any substantial difference in spectral tuning for S+ and S− is illustrated by the right-hand plots being essentially flattened versions, with nearly the same orientations, of the surfaces in the left-hand plots.

The L- and M-cone contrast weights in Table 2 have dissimilar magnitudes, with about twice as great a weight for M cones. This difference in L and M magnitudes indicates that these field sensitivities do not represent cardinal-like, R (L–M, approximately) and G (M–L, approximately) detection mechanisms, which have L- and M-cone contrast weights that are almost exactly the negative of one another (Eskew, 2008; Eskew et al., 1999). The signs, but not the magnitudes, of the weights are suggestive of red/green *hue* mechanisms (see General discussion).

Rod controls

There are known differences between rod increment and decrement sensitivities (Patel & Jones, 1968), and there is substantial rod input to the small bistratified ganglion cells that carry S-ON signals, at least in peripheral retina (Field et al., 2009). Even though the mean brightness of our monitor was near rod saturation levels, we remeasured some of the EvNs after a 90% rod bleach. The asymmetry between S+ and S− tests was preserved, showing that the differences in

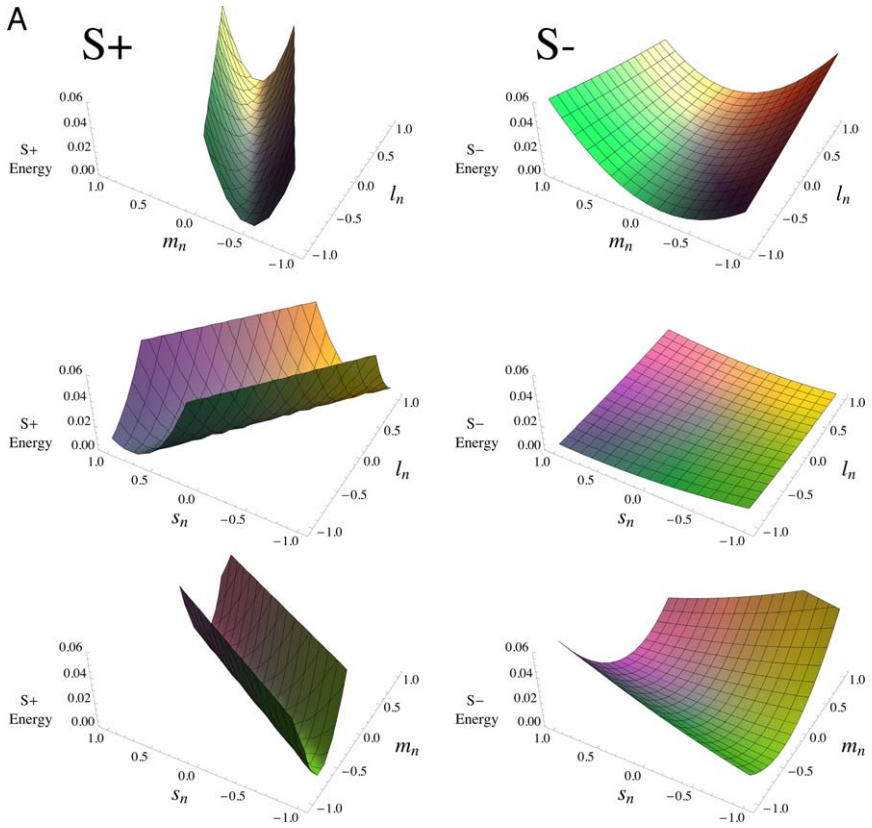

Figure 5. Cone combination model. Plot of the linear mechanism model for noise masking (Equation 3), using the parameter values given in Table 2. Panel (A) is for QW; (B) is for DR. S+ tests are on the left, and S– tests are on the right; the three rows in each panel represent the effects of noises in the (L,M), (L,S), and (M,S) planes of cone contrasts, respectively. The scales are the same in each panel, with the surfaces truncated when they reach the top of the (invisible) bounding box containing the plot. The plots cover the full range of cone contrasts, to better illustrate the shapes of the model surfaces, rather than the more limited monitor gamut range. The surfaces have been colored to approximately represent the chromaticities of the noise (i.e., two points that are symmetric about the origin depict the two chromaticities of the binary noise).

test polarity could not be due to rod intrusion. Details are described in Appendix B.

General discussion

There are four main results from the present study. First, various chromatic noises masked S-cone increments to a much greater degree than S-cone decrements. We did not find any noise color direction that produced more masking of S– than S+ tests, and only for achromatic noise were they approximately equal. Second, the L–M and M noises produced steeper EvNs for both S+ and S– tests than did S-cone noise itself; for S– tests, L cones also produced a greater masking effect than S cones. Third, there is no evidence in these data of a spectral difference in the long-wave signals that mask S+ and S– tests. Fourth, the pattern of masking across noise chromaticities is well approximated by a linear cone combination, with opposed L- and M-cone inputs.

More masking of S+ than S–

This first result is consistent with reports that in the LGN, S-ON cells have greater gain to S-cone modulations than S-OFF cells (Solomon & Lennie, 2005; Tailby, Solomon, & Lennie, 2008; Tailby, Szmajda et al., 2008). It could also be consistent with some reports of response saturation and/or contrast gain control in S-ON but not in S-OFF cells at the level of the LGN (Solomon & Lennie, 2005; Tailby, Solomon, Dhruv, & Lennie, 2008), if much of the masking results from contrast gain mechanisms rather than by additive noise. However, these saturation/gain control differences have not been consistently found in the LGN (Tailby, Solomon, & Lennie, 2008; Tailby, Szmajda et al., 2008) or cortex (Solomon & Lennie, 2005), and more contrast adaptation has been reported

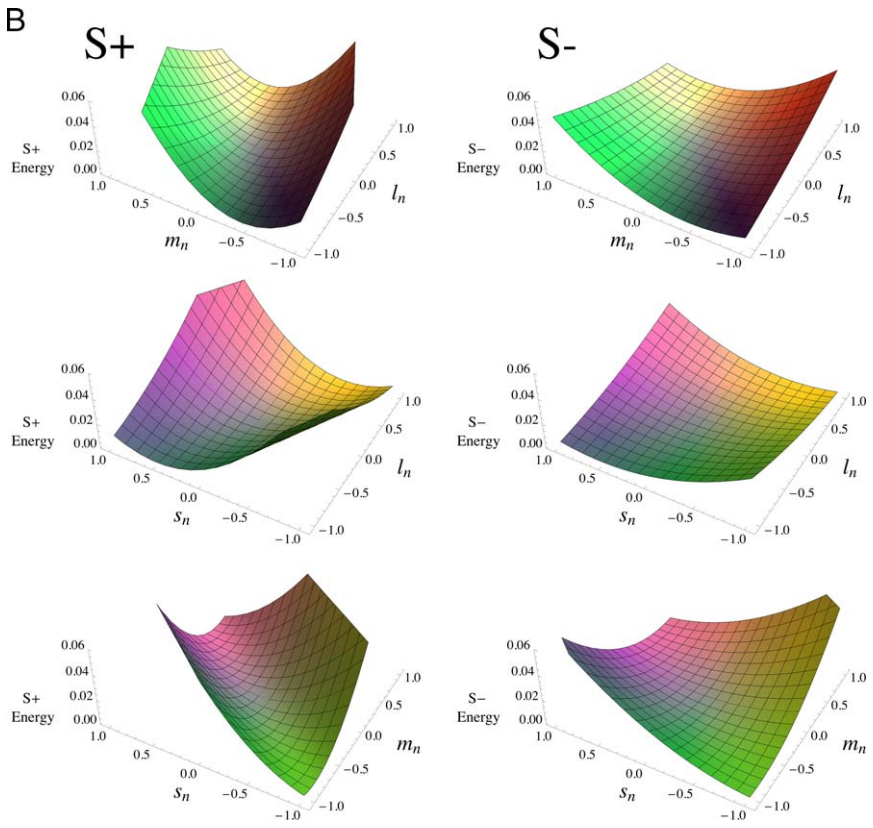

Figure 5. Continued

for S-OFF than S-ON LGN cells (Tailby, Solomon, & Lennie, 2008).

Psychophysically, the greater S+ masking implies that the S+ and S– mechanisms are asymmetric, in the sense that they do not differ merely in the polarity of their cone contributions. No symmetric pair of mechanisms, whether they are linear or nonlinear, can have different amounts of masking produced by the identical noise stimulus (Appendix C). Thus, these two stimuli are detected by distinct, unipolar psychophysical mechanisms (Eskew, 2008, 2009). The two mechanisms must differ in the strengths of their cone inputs, the types of nonlinearities (including contrast gain control), or their spatiotemporal integration properties (and thus their sampling efficiencies; Pelli, 1990). Although differences in spatial and temporal integration for S+ and S– tests have been found in peripheral vision (Murzac, Vassilev, & Zlatkova, 2003; Newton & Eskew, 2001; Vassilev et al., 2003; Zlatkova et al., 2008), few such differences have been found in the central 10° (the temporal impulse responses estimated by Shinomori & Werner, 2008, are exceptions), so if integration differences are responsible for the large differences in masking of our near-foveal tests, the cause would likely be greater integration of the peripheral parts of the *noise* stimulus by the S+ compared to the S– mechanism, rather than less integration of the *test* by the S– compared to the S+ mechanism. Tests of this idea would require varying the spatiotemporal properties of the stimuli, which was not done here.

Vingrys and Mahon (1998) studied pedestal-masking effects on S+ and S– tests. An S– pedestal produced less masking of S– tests than an S+ pedestal did on S+ tests (see also Gabree & Eskew, 2006). Differences in pedestal masking would not be easily explained by differences in spatiotemporal integration, since the pedestal and test had the same shape and time course. However, like the present results, these findings are consistent with lesser contrast gain control in S– pathways.

Alone of the noises we tested, achromatic (L+M+S) noise does not produce different masking for S+ and S– tests. This might simply be due to the weaker effect of this noise; however, the maximal achromatic noise raised energy thresholds by at least five-fold. Note that adding L and M noise components in phase with an S component greatly reduces the amount of masking of both S+ and S– tests (compare Figure 4, "S" vs. "A" slopes). The lesser achromatic masking suggests that most of the masking effects result from cone-antagonistic inputs, as indicated by the cone weights in Table 2.

Many chromatic detection studies use bipolar stimuli, such as S-cone gratings or S-cone flicker, which

have both increment and decrement components. The higher thresholds for unipolar S+ stimuli indicate that responses to bipolar stimuli may be dominated by their S– components; this "S– dominance" would be small at the luminance levels typically used with monitors (McLellan & Eskew, 2000, figure 3), but would grow with luminance. S– dominance would be especially large when masking stimuli are used to raise thresholds, as shown here. Thus many studies of S-cone acuity (e.g., Humanski & Wilson, 1992), equiluminant chromatic detection (e.g., Eskew, Newton, & Giulianini, 2001; Hansen & Gegenfurtner, 2006) and S-cone flicker (e.g., McKeefry, Murray, & Kulikowski, 2001) may be primarily measuring the S– response. The inverted sign of the S-cone input to luminance flicker (Stockman, MacLeod, & DePriest, 1991), seen on long-wavelength backgrounds, may be consistent with S– dominance: only the decremental component may be detectable in the flicker, especially under steady long-wave adaptation (McLellan & Eskew, 2000).

L–M and M masking of S+ and S–

The second main result—that L–M- and M-cone noises produced more masking than S-cone noise (Figure 4)—was unexpected. It implies that long-wave cone inputs to these detection mechanisms are stronger than the S-cone inputs, and again that a major component of the masking signal is carried via L- and M-cone antagonism. These effects appear in the estimated cone weights in Table 2, and in the top rows of Figure 5a and b. The large masking by L and M means that a noise vector pointed far off from the S-cone axis in cone space can have a large effect on S-cone detection. This finding is consistent with results of Eskew et al. (2001), who found that noise along the L–M direction of the equiluminant plane produced substantial masking of S-cone tests, and of Singer and D'Zmura (1994), who found substantial contrast induction into S-cone patterns from L–M and achromatic surrounding patterns. This result is not consistent with the simple cardinal axis framework, known to be wrong in other contexts as well (Eskew, 2009; Hansen & Gegenfurtner, 2013; Krauskopf, 1999).

In the outer retina, a L+M signal that opposes S cones is generated in at least two ways (reviewed in Dacey et al., 2014): (a) H2 horizontal cells provide feedback to the S cones, generating a chromatically and spatially opponent surround in the S cones themselves, and (b) the small bistratified cell opposes S-ON cells against DB2 diffuse bipolar signals. Neither of these pathways could provide the L–M opponent signal seen so clearly in the present data and in the previous psychophysical results just summarized; the long-wave signals observed here likely have a cortical origin.

In many psychophysical models, including the cardinal axis model, the signal that opposes S-cone signals is assumed to be a sum of L and M (Cole, Hine, & McIlhagga, 1993, 1994; Eskew et al., 1999; Krauskopf et al., 1982; Sankeralli & Mullen, 1996; Shapiro & Zaidi, 1992; Thornton & Pugh, 1983; Zaidi, Shapiro, & Hood, 1992). However, other results suggest this signal is not simply a sum, but instead includes cone-opponent terms (Guth, 1991; McLellan & Eskew, 2000; Wisowaty, 1983). The color model of De Valois and De Valois (1993) has L–M and L+M components opposing the S signal; these long-wave components are embedded in consecutive stages of signal combinations. The present finding is consistent with these latter results.

Similar long wave inputs for S+ and S–

There are several reports of differences in the long-wave cone contributions to the populations of S-ON and S-OFF cells in the LGN and visual cortex. The S signal in S-ON cells is more likely have both L and M cones opposing it, while S-OFF cells often have a combination of S and M cones opposing L cones (Chatterjee & Callaway, 2003; Solomon & Lennie, 2005; Tailby, Solomon, & Lennie, 2008). However, it is not clear how these population differences would be reflected in psychophysical noise masking performance, which is likely to be dominated by the most sensitive subset of cells in a given condition.

Psychophysically, McLellan & Eskew (2000) clearly demonstrated a relative difference in spectral sensitivity to transient tritanopia for these two test polarities (in color normal observers), with S+ thresholds having higher field sensitivity to long-wavelength lights; in their (nonlinear) model, there was effectively greater L cone opposition to S+ than S– signals. However, in the present study the relative cone weights (Table 2) are nearly identical for the two test polarities. Perhaps the S-ON and S–OFF pathways that are most sensitive under steady-state conditions, rather than transient ones, have similar long-wave inputs.

Linear chromatic mechanism

The third result, the linear cone combination, was also unexpected. Giulianini and Eskew (2007), using a novel noise superposition method, clearly showed that no linear model could account for noise masking of S+ or S– tests. There are only two substantial stimulus differences between that study and the present one: (a) the present test stimulus was a blurred annulus rather than the Gaussian blob used in the earlier study, and (b) the noise rings filled the entire screen in the present

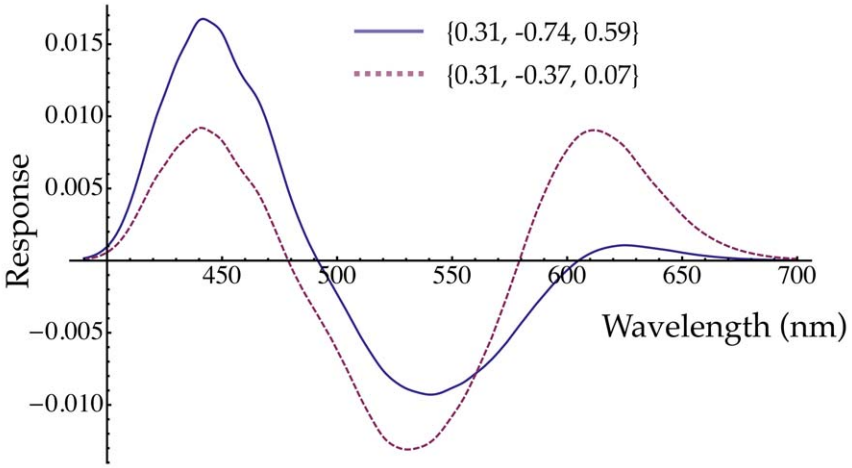

Figure 6. Red-green valence functions. The solid line was calculated using the DR S+ weights from Table 2, assuming an equal energy "white" background and equal energy increment tests of the given wavelength (cf. Takahashi et al., 1985, who used a steady white background and briefly flashed monochromatic tests to which adaptation would be minimal or zero, as assumed here for the cone contrast calculations). The zero crossings are too long in wavelength to account for unique blue and unique yellow. For the dashed line, the M weight was halved and the S weight was divided by 8. These adjustments make the zero crossings near 479 and 579 nm.

study, rather than being confined to the region of the screen near the test.

The noise superposition study was specifically designed to test for linearity, whereas the present study was primarily designed to compare S+ and S– detection. A larger number of different noise chromaticities were used for the noise superposition experiment, and in some of these chromatic directions (e.g., the L–M direction, the only noise common to both studies and all observers), detection performance was fairly close to the linear prediction. Thus the two sets of results may not be in direct conflict. The linear model used here is likely to be only an approximation, but it is an excellent approximation for the present conditions, accounting for a minimum of 89% of the variance (Table 2).

For both S+ and S– tests, the approximately-linear model (Equation 3, Table 2) has opposed L and M cone inputs, with the S-cone input being of the same sign as the L cone one (Hurvich & Jameson, 1957; Stockman & Brainard, 2009; Wuerger, Atkinson, & Cropper, 2005). Cortical S-OFF responses have more often been found to align with the M cone signal, compared to S-ON responses (Conway, 2001; Solomon & Lennie, 2005); neither the S+ or S– weights in Table 2 shows this pattern. Instead, the pattern of signs is suggestive of a red/green *hue* mechanism, in which the S-cone component, having the same sign as the L cones, creates short-wavelength redness (whether cone combination in hue mechanisms is actually linear is beyond the scope of the present paper; see, for example, Ingling, 1977). Although the pattern of signs suggests red and green mechanisms, the magnitudes of the weights do not: both the M- and S-cone contributions estimated here are too large for a linear hue mechanism. This point is illustrated in Figure 6, in which the response of a mechanism with DR's S+ cone contrast weights to monochromatic increment lights is plotted as the solid line. The shape, specifically the zero crossings (unique hues), of the hypothetical hue mechanism response is not like measured hue valence functions (e.g., Hurvich & Jameson, 1957; Takahashi, Ejima, & Akita, 1985): both the M- and S-cone weights are too large, relative to the L-cone weight. The dashed line in Figure 6 illustrates the function after the M and S weights are divided by 2 and 8, respectively; in this case the zero crossings are approximately correct for unique blue and unique yellow wavelengths. Thus if the S+ and S– mechanisms estimated here are actually linear, they are not red and green hue mechanisms, even though they have some superficial similarity to them, because the M and especially the S-cone weights are too large.

Conclusion

Whereas most cone contrast modulations below about 15 Hz are detected by symmetric R and G mechanisms, the pathways fed by S-cone increment and decrement signals differ in numerous ways (Gabree & Eskew, 2006; Krauskopf et al., 1986; McLellan & Eskew, 2000; Shapiro & Zaidi, 1992; Shinomori et al., 1999; Shinomori & Werner, 2008; Vassilev et al., 2003; Vassilev et al., 2000; Vingrys & Mahon, 1998; Zlatkova et al., 2008), including the large noise masking differences found in the present study. The linear cone combination weights (Table 2), and the approximately

constant log difference between the S+ and S– slopes for the chromatic noises (Figure 4) strongly suggest that, in the presence of chromatic noises, the S+ and S– detection mechanisms differ, not in their relative spectral characteristics, but in terms of contrast sensitivity, most likely due to greater contrast gain control in S+ mechanisms.

Keywords: S cone, on/off, increment/decrement, color mechanisms, chromatic detection, chromatic noise

Acknowledgments

Supported by EY09712 from the NIH and BCS-1353338 from the NSF. The authors are grateful for the detailed and insightful comments on the manuscript provided by Dr. Barry Lee, and especially by Dr. Andrew Stockman, and for expert help from Mr. Timothy Shepard.

* Current address for Quanhong Wang: Faculty of Psychology, MoE Southwest University, Chongqing, China.
Commercial relationships: none.
Corresponding author: Rhea T. Eskew, Jr.
Email: eskew@neu.edu.
Address: Northeastern University, Psychology Department, Boston, MA USA.

References

Bosten, J. M., Bargary, G., Goodbourn, P. T., Hogg, R. E., Lawrance-Owen, A. J., & Mollon, J. D. (2014). Individual differences provide psychophysical evidence for separate on- and off-pathways deriving from short-wave cones. *Journal of the Optical Society of America A: Optics, Image Science, and Vision, 31*(4), A47–54. doi:10.1364/JOSAA.31.000A47.

Chaparro, A., Stromeyer, C. F., III, Chen, G., & Kronauer, R. E. (1995). Human cones appear to adapt at low light levels: measurements on the red-green detection mechanism. *Vision Research, 35*(22), 3103–3118.

Chatterjee, S., & Callaway, E. M. (2003). Parallel colour-opponent pathways to primary visual cortex. *Nature, 426*(6967), 668–671.

Cole, G. R., Hine, T., & McIlhagga, W. (1993). Detection mechanisms in L-, M-, and S-cone contrast space. *Journal of the Optical Society of America A, 10*(1), 38–51.

Cole, G. R., Hine, T. J., & McIlhagga, W. (1994). Estimation of linear detection mechanisms for stimuli of medium spatial frequency. *Vision Research, 34*(10), 1267–1278.

Conway, B. R. (2001). Spatial structure of cone inputs to color cells in alert macaque primary visual cortex (V-1). *Journal of Neuroscience, 21*(8), 2768–2783.

Curcio, C. A., Allen, K. A., Sloan, K. R., Lerea, C. L., Hurley, J. B. , Klock, I. B., & Milam, A. H. (1991). Distribution and morphology of human cone photoreceptors stained with anti-blue opsin. *The Journal of Comparative Neurology, 312*(4), 610–624.

Dacey, D. M. (1996). Circuitry for color coding in the primate retina. *Proceedings of the National Academy of Sciences, USA, 93*(2), 582–588.

Dacey, D. M., Crook, J. D., & Packer, O. S. (2014). Distinct synaptic mechanisms create parallel S-ON and S-OFF color opponent pathways in the primate retina. *Visual Neuroscience, 31*(2), 139–151. doi:10.1017/S0952523813000230.

Dacey, D. M., & Lee, B. B. (1994). The "blue-on" opponent pathway in primate retina originates from a distinct bistratified ganglion cell type. *Nature, 367*(6465), 731–735.

Dacey, D. M., & Packer, O. S. (2003). Colour coding in the primate retina: Diverse cell types and cone-specific circuitry. *Current Opinion in Neurobiology, 13*(4), 421–427.

Dacey, D. M., Peterson, B. B., Robinson, F. R., & Gamlin, P. D. (2003). Fireworks in the primate retina: In vitro photodynamics reveals diverse LGN-projecting ganglion cell types. *Neuron, 37*(1), 15–27.

De Valois, R. L., & De Valois, K. (1993). A multi-stage color model. *Vision Research, 33*(8), 1053–1065.

Eskew, R. T., Jr. (2008). Chromatic detection and discrimination. In R. H. Masland & T. D. Albright (Eds.), *The senses: A comprehensive reference. (Vol. 2: Vision II;* pp. 101–117). New York: Academic Press.

Eskew, R. T., Jr. (2009). Higher order color mechanisms: A critical review. *Vision Research, 49*(22), 2686–2704. doi:10.1016/j.visres.2009.07.005.

Eskew, R. T., Jr., McLellan, J. S., & Giulianini, F. (1999). Chromatic detection and discrimination. In K. R. Gegenfurtner & L. T. Sharpe (Eds.), *Color vision: From genes to perception* (pp. 345–368). Cambridge, UK: Cambridge University Press.

Eskew, R. T., Jr., Newton, J. R., & Giulianini, F. (2001). Chromatic detection and discrimination analyzed by a Bayesian classifier. *Vision Research, 41*(7), 893–909. doi:S0042-6989(00)00298-4 [pii].

Field, G. D., Greschner, M., Gauthier, J. L., Rangel, C., Shlens, J., Sher, A., ... Chichilnisky, E. J. (2009). High-sensitivity rod photoreceptor input to the blue-yellow color opponent pathway in macaque retina. *Nature Neuroscience, 12*(9), 1159–1164. doi:10.1038/nn.2353.

Gabree, S. H., & Eskew, R. T., Jr. (2006). Pedestal masking of S-cone increments and decrements: Less contrast gain control in the S-OFF pathways. *Journal of Vision, 6*(13):7, http://www.journalofvision.org/content/6/13/7, doi:10.1167/6.13.7. [Abstract]

Gegenfurtner, K. R., & Kiper, D. C. (1992). Contrast detection in luminance and chromatic noise. *Journal of the Optical Society of America A, 9*(11), 1880–1888.

Giulianini, F., & Eskew, R. T., Jr. (1998). Chromatic masking in the (delta L/L, delta M/M) plane of cone-contrast space reveals only two detection mechanisms. *Vision Research, 38*(24), 3913–3926. doi:S0042-6989(98)00068-6 [pii].

Giulianini, F., & Eskew, R. T., Jr. (2007). Theory of chromatic noise masking applied to testing linearity of S-cone detection mechanisms. *Journal of the Optical Society of America A, Optics, Image Science, and Vision, 24*(9), 2604–2621. doi:10.1364/JOSAA.24.002604.

Guth, S. L. (1991). Model for color vision and light adaptation. *Journal of the Optical Society of America, 8*(6), 976–993.

Hansen, T., & Gegenfurtner, K. R. (2006). Higher level chromatic mechanisms for image segmentation. *Journal of Vision, 6*(3):5, 239–259, http://www.journalofvision.org/content/6/3/5, doi:10.1167/6.3.5. [PubMed] [Article]

Hansen, T., & Gegenfurtner, K. R. (2013). Higher order color mechanisms: Evidence from noise-masking experiments in cone contrast space. *Journal of Vision, 13*(1):26, 1–21, http://www.journalofvision.org/content/13/1/26, doi:10.1167/13.1.26. [PubMed] [Article]

Hood, D. C., & Finkelstein, M. A. (1986). Sensitivity to light. In K. R. Boff, L. Kaufman, & J. P. Thomas (Eds.), *Handbook of perception and human performance. Volume 1: Sensory processes and perception, Vol. 1* (Chapter 5, pp. 1–66). New York: Wiley.

Humanski, R. A., & Wilson, H. R. (1992). Spatial frequency mechanisms with short-wavelength-sensitive cone inputs. *Vision Research, 32*(3), 549–560.

Hurvich, L. M., & Jameson, D. (1957). An opponent-process theory of color vision. *Psychological Review, 64*(6), 384–404.

Ingling, C. R. (1977). The spectral sensitivity of the opponent-color channels. *Vision Research, 17,* 1083–1089.

Klug, K., Herr, S., Ngo, I. T., Sterling, P., & Schein, S. (2003). Macaque retina contains an S-cone OFF midget pathway. *Journal of Neuroscience, 23*(30), 9881–9887.

Klug, K., Tsukamoto, Y., Sterling, P., & Schein, S.J. (1993). Blue cone off-midget ganglion cells in macaque. *Investigative Ophthalmology & Visual Science (Suppl.), 34,* 986.

Kouyama, N., & Marshak, D. W. (1992). Bipolar cells specific for blue cones in the macaque retina. *Journal of Neuroscience, 12*(4), 1233–1252.

Krauskopf, J. (1999). Higher order color mechanisms. In K. R. Gegenfurtner & L. T. Sharpe (Eds.), *Color vision: From genes to perception*. Cambridge, UK: Cambridge University Press.

Krauskopf, J., Williams, D. R., & Heeley, D. W. (1982). Cardinal directions of color space. *Vision Research, 22*(9), 1123–1131.

Krauskopf, J., Williams, D. R., Mandler, M. B., & Brown, A. M. (1986). Higher order color mechanisms. *Vision Research, 26*(1), 23–32.

Kuffler, S. W. (1953). Discharge patterns and functional organization of mammalian retina. *Journal of Neurophysiology, 16*(1), 37–68.

Legge, G. E., Kersten, D., & Burgess, A. E. (1987). Contrast discrimination in noise. *Journal of the Optical Society of America A, 4*(2), 391–404.

Lu, Z. L., & Dosher, B. A. (2008). Characterizing observers using external noise and observer models: Assessing internal representations with external noise. *Psychological Review, 115*(1), 44–82. doi:10.1037/0033-295X.115.1.44.

Mariani, A. P. (1984). Bipolar cells in monkey retina selective for the cones likely to be blue-sensitive. *Nature, 308*(5955), 184–186.

McKeefry, D. J., Murray, I. J., & Kulikowski, J. J. (2001). Red-green and blue-yellow mechanisms are matched in sensitivity for temporal and spatial modulation. *Vision Research, 41*(2), 245–255.

McLellan, J. S., & Eskew, R. T., Jr. (2000). ON and OFF S-cone pathways have different long-wave cone inputs. *Vision Research, 40*(18), 2449–2465. doi: 10/1016.S0042-6989(00)00107-3.

Murzac, A., Vassilev, A., & Zlatkova, M. (2003). Temporal summation of S-cone ON- and OFF-signals in the central the peripheral human retina.

Comptes Rendus de l'Académie Bulgare des Sciences, 56(12), 93–96.

Newton, J. R., & Eskew, R. T., Jr. (2001). Peripheral chromatic contrast sensitivity functions differ for S-cone increment, S-cone decrement, red and green patterns. *Investigative Ophthalmology & Visual Science (Suppl.), 42*(4), S97.

Patel, A. S., & Jones, R. W. (1968). Increment and decrement visual thresholds. *Journal of the Optical Society of America, 58*(5), 696–699.

Pelli, D. G. (1990). The quantum efficiency of vision. In C. Blakemore (Ed.), *Vision: Coding and efficiency* (pp. 3–24). Cambridge, UK: Cambridge University Press.

Pelli, D. G., & Zhang, L. (1991). Accurate control of contrast on microcomputer displays. *Vision Research, 31*(7–8), 1337–1350.

Sankeralli, M. J., & Mullen, K. T. (1996). Estimation of the L-, M-, and S-cone weights of the postreceptoral detection mechanisms. *Journal of the Optical Society of America A, 13*(5), 906–915.

Schiller, P. H. (1992). The ON and OFF channels of the visual system. *Trends in Neuroscience, 15*(3), 86–92.

Shapiro, A. G., & Zaidi, Q. (1992). The effects of prolonged temporal modulation on the differential response of color mechanisms. *Vision Research, 32*(11), 2065–2075.

Shinomori, K., Spillmann, L., & Werner, J. S. (1999). S-cone signals to temporal OFF-channels: asymmetrical connections to postreceptoral chromatic mechanisms. *Vision Research, 39*(1), 39–49.

Shinomori, K., & Werner, J. S. (2008). The impulse response of S-cone pathways in detection of increments and decrements. *Visual Neuroscience, 25*(3), 341–347. doi:10.1017/S0952523808080218.

Singer, B., & D'Zmura, M. (1994). Color contrast induction. *Vision Research, 34*(23), 3111–3126.

Smithson, H. E. (2014). S-cone psychophysics. *Visual Neuroscience, 31*(2), 211–225. doi:10.1017/S0952523814000030.

Solomon, S. G., & Lennie, P. (2005). Chromatic gain controls in visual cortical neurons. *Journal of Neuroscience, 25*(19), 4779–4792.

Stockman, A., & Brainard, D. H. (2009). Color vision mechanisms. In M. Bass, C. DeCusatis, J. M. Enoch, V. Lakshminarayanan, G. Li, C. Macdonald, V. Mahajan, & E. van Stryland (Eds.), *The Optical Society of America Handbook of Optics (3rd ed.)*. New York: McGraw Hill.

Stockman, A., MacLeod, D. I. A., & DePriest, D. D. (1991). The temporal properties of the human short-wave photoreceptors and their associated pathways. *Vision Research, 31*(2), 189–208.

Stockman, A., & Sharpe, L. T. (2000). The spectral sensitivities of the middle- and long-wavelength-sensitive cones derived from measurements in observers of known genotype. *Vision Research, 40*(13), 1711–1737.

Stromeyer, C. F., III, Cole, G. R., & Kronauer, R. E. (1985). Second-site adaptation in the red-green chromatic pathways. *Vision Research, 25*(2), 219–237.

Tailby, C., Solomon, S. G., Dhruv, N. T., & Lennie, P. (2008). Habituation reveals fundamental chromatic mechanisms in striate cortex of macaque. *Journal of Neuroscience, 28*(5), 1131–1139. doi:10.1523/JNEUROSCI.4682-07.2008.

Tailby, C., Solomon, S. G., & Lennie, P. (2008). Functional asymmetries in visual pathways carrying S-cone signals in macaque. *Journal of Neuroscience, 28*(15), 4078–4087. doi:10.1523/JNEUROSCI.5338-07.2008.

Tailby, C., Szmajda, B. A., Buzas, P., Lee, B. B., & Martin, P. R. (2008). Transmission of blue (S) cone signals through the primate lateral geniculate nucleus. *Journal of Physiology, 586*(Pt 24), 5947–5967. doi:10.1113/jphysiol.2008.161893.

Takahashi, S., Ejima, Y., & Akita, M. (1985). Effect of light adaptation on the perceptual red-green and yellow-blue opponent-color responses. *Journal of the Optical Society of America A, 2*(5), 705–712.

Thomas, M. M., & Lamb, T. D. (1999). Light adaptation and dark adaptation of human rod photoreceptors measured from the a-wave of the electroretinogram. *Journal of Physiology, 518*(Pt 2), 479–496. doi:10.1111/j.1469-7793.1999.0479p.x.

Thornton, J. E., & Pugh, E. N., Jr. (1983). Relationship of opponent-colours cancellation measures to cone-antagonist signals deduced from increment threshold data. In J. D. Mollon & L. T. Sharpe (Eds.), *Colour vision: Physiology and psychophysics* (pp. 361–373). London: Academic.

Vassilev, A., Mihaylova, M. S., Racheva, K., Zlatkova, M., & Anderson, R. S. (2003). Spatial summation of S-cone ON and OFF signals: Effects of retinal eccentricity. *Vision Research, 43*(27), 2875–2884.

Vassilev, A., Zlatkova, M., Manahilov, V., Krumov, A., & Schaumberger, M. (2000). Spatial summation of blue-on-yellow light increments and decrements in human vision. *Vision Research, 40*(8), 989–1000.

Vingrys, A. J., & Mahon, L. E. (1998). Color and luminance detection and discrimination asymme-

tries and interactions. *Vision Research, 38*(8), 1085–1095.

Watson, A. B. (1979). Probability summation over time. *Vision Research, 19*(5), 515–522.

Webster, M. A., & Mollon, J. D. (1994). The influence of contrast adaptation on color appearance. *Vision Research, 34*(15), 1993–2020.

Williams, D. R. MacLeod, D. I. A., & Hayhoe, M. M. (1981). Foveal tritanopia. *Vision Research, 21*(9), 1341–1356.

Wisowaty, J. J. (1983). An action spectrum for the production of transient tritanopia. *Vision Research, 23*(8), 769–774.

Wuerger, S. M., Atkinson, P., & Cropper, S. (2005). The cone inputs to the unique-hue mechanisms. *Vision Research, 45*(25–26), 3210–3223.

Zaidi, Q., Shapiro, A., & Hood, D. (1992). The effect of adaptation on the differential sensitivity of the S-cone color system. *Vision Research, 32*(7), 1297–1318.

Zlatkova, M. B., Vassilev, A., & Anderson, R. S. (2008). Resolution acuity for equiluminant gratings of S-cone positive or negative contrast in human vision. *Journal of Vision, 8*(3):9, 1–10, http://www.journalofvision.org/content/8/3/9, doi:10.1167/8.3.9. [PubMed] [Article]

Appendix A: Units

Test cone contrast energy

Both the test and the noise are treated in one spatial dimension (the radial one). The contrast energy in the unit-contrast test is $\int_{-\infty}^{+\infty}\left(0.7584e^{\frac{-r^2}{2}}\left(1-Cos(\pi r)\right)\right)^2 dr = 1.3562$ deg. Multiplying by the duration of the test flash produces a constant of proportionality of $Q_t = 0.2712$ deg·sec. The S-cone contrast produced by the test (after halving the nominal, peak value to account for the half-toning) was squared and multiplied by this constant to calculate the test energy E_t.

Noise cone contrast power

The power spectrum of the noise (at unit contrast) is the product of the squared-moduli of the spatial and temporal Fourier transforms of the noise sampling functions:

$$Q_n(\omega_r,\omega_t) = \left(\overline{\Theta(\omega_r)\Theta^*(\omega_r)}\right)\left(\overline{\Gamma(\omega_t)\Gamma^*(\omega_t)}\right)$$

(see Legge, Kersten, & Burgess, 1987). Both sampling functions are unit rectangular windows, with widths $\Delta r = 0.04$ deg (two pixels) and $\Delta t = .0533$ sec (every fourth monitor refresh), and their transforms Θ and Γ are sinc functions (see Equation 4, below). This spatio-temporal spectrum must be multiplied by the contrast variance $\overline{c^2(j\Delta r, i\Delta t)}$ of the binary noise, which, for unit contrast, is $(.25)(-1)^2 + (.50)(0)^2 + (.25)(1)^2 = 1/2$ (by the definition of variance of a discrete binary random variable, and including the half-toning). The value of this variance over 1° × 1 sec is therefore

$$\sum_{j=-\frac{1}{2}\left(\frac{1}{\Delta r}-1\right)}^{\frac{1}{2}\left(\frac{1}{\Delta r}-1\right)}\sum_{i=0}^{\frac{1}{\Delta t}-1}\overline{c^2(j\Delta r, i\Delta t)} = \frac{1}{2}\frac{1}{\Delta r\Delta t}$$

Thus, the contrast power spectrum is

$$Q_n(\omega_r,\omega_t) = \left[(\Delta r)^2 sinc^2\left(\frac{2\pi\omega_r\Delta r}{2}\right)\right] \times \left[(\Delta t)^2 sinc^2\left(\frac{2\pi\omega_t\Delta t}{2}\right)\right]\left[\frac{1}{2\Delta r\Delta t}\right] \quad (4)$$

in units of [deg^2] [sec^2] [deg^{-1}·sec^{-1}] = deg·sec, commensurate with the test energy. This function is plotted in the bottom panels of Figure 2. The value at DC, $Q_n(0,0) \equiv Q_n = \frac{1}{2}\Delta r\Delta t = 1.07 \times 10^{-3}$ deg·sec, was used as the proportionality between squared-contrast (cone contrast vector length) and noise power.

Appendix B: Rod controls

The steady monitor background was approximately 3.15 log scot Td (radiometrically calibrated), near rod saturation (Hood & Finkelstein, 1986). However, because there are known differences between rod increment and decrement sensitivities (Patel & Jones, 1968), we ran several conditions to be certain that rods were not intruding, and that the asymmetry we report here persisted after a rod bleach. The rod control experiments were run several months after the main experiment. We performed a bleach with a field diameter of about 10° and duration of 10 s, consisting of 7.4 log sct Td · s of "white" light (radiometrically calibrated). This light was calculated to isomerize more than 90% of rhodopsin (Thomas & Lamb, 1999), enough to substantially raise rod thresholds.

To trace the time course of bleaching recovery and determine the period during which data would be collected in the main rod bleach experiment, one observer set method of adjustment thresholds after bleaching. Flashes occurred every 1.5 s, and the observer used buttons to adjust the contrast; when he

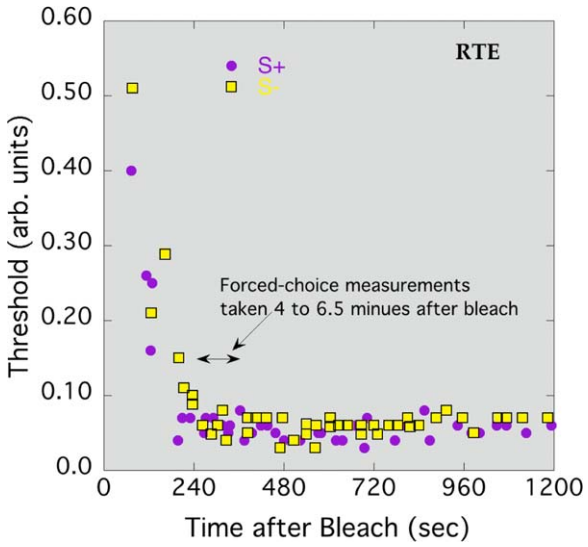

Figure 7. Method of adjustment thresholds for S– (squares) and S+ (circles) tests, following a 90% rod bleach at time 0. Observer RTE.

was satisfied, the threshold contrast and the time since the bleach were recorded. Figure 7 shows thresholds for S+ and S– tests, pooled from two runs, as a function of time after the rod bleach. Thresholds fell rapidly over the first three minutes, and neared asymptote by about four minutes.

In Figure 7, there is no evidence of a second branch in the threshold curve, suggesting that the white monitor background alone was sufficient to desensitize the rods to these tests. However, these method of adjustment results are not completely conclusive; the observer might have unintentionally used the hue of the stimuli to set thresholds. Moreover, no noise was present in the method of adjustment experiment. For these reasons, some of the EvNs were remeasured after the rod bleach, using the following procedure. After 10 s of bleaching and then 15 s pause in a dark room, the observer started adapting for 4 minutes to the white monitor background (with or without masking noise) to reach the cone plateau. This was followed by 75 2AFC trials lasting less than 2.5 minutes (covering the time window marked by the double-arrow in Figure 7). S+ and S– detection thresholds were measured along with the L and M cone noises (observer QW) or S-cone noise (observers DR and RTE).

Table 3 provides slopes of S+ and S– EvNs after a rod bleach. In every case the S+ function is steeper than the S–, and in most cases the magnitudes of the slopes are similar to those measured without the rod bleach. Thus, the main results are unlikely to have been contaminated in any significant way by rod intrusion; the asymmetry is seen in S-cone pathways.

Noise	Observer	Test	EvN slope (*SE*)
L	QW	S+	108.2 (3.1)
		S–	14.3 (8.0)
M	QW	S+	138.1 (1.9)
		S–	22.4 (0.4)
S	DR	S+	1044.1 (88.9)
		S–	793.0 (197.0)
S	RTE	S+	65.3 (12.4)
		S–	34.5 (9.1)

Table 3. Noise masking slopes after a 90% rod bleach, with standard errors.

Appendix C: EvN functions and mechanism energy and power

The EvN of Equation 1 is cast in terms of the proximal stimuli: the cone contrast energy and power as seen at the level of the photoreceptors. Giulianini and Eskew (2007) studied the relationship between the energy of a stimulus at threshold and the contrast power of a masking noise, not in terms of the stimulus, but rather in terms of the effects of the stimuli within a psychophysical detection mechanism: the "mechanism energy" produced by the test stimulus and the "mechanism noise" produced by the masking noise. This change effectively moves the relationship between test and noise further inside the visual system, and is therefore necessarily more theoretical than the empirical EvN itself. Here we derive the mechanism energy and mechanism noise for the present case.

A test stimulus is defined in terms of a vector $\mathbf{v}$ of three cone contrasts l, m, and s varying in space and time. The chromatic detection mechanism, which may be a linear or nonlinear combination of the cone contrasts, is written as the function f, so the mechanism response to a stimulus vector $\mathbf{v}$ is defined as

$$f(\mathbf{v}) = f\begin{bmatrix} l_t(x,y,z) \\ m_t(x,y,z) \\ s_t(x,y,z) \end{bmatrix}$$

(with t indicating test and z being time) Assuming that the cone combination f is independent of space and time (i.e., it is chromo-separable, Giulianini & Eskew, 2007), we may factor out the space-time function $q(x,y,z)$ from the chromatic function $f(l,m,s)$ and write the mechanism energy as

$$\begin{aligned} E[Mech(\mathbf{v})] &= \iiint f^2(l_t,m_t,s_t)q^2(x,y,z)dxdydz \\ &= f^2(l_t,m_t,s_t)\iiint q^2(x,y,z)dxdydz \\ &= f^2(l_t,m_t,s_t)Q_t. \end{aligned} \quad (5)$$

The mechanism noise may be expressed analogously (Giulianini & Eskew, 2007), as

$$E[Mech(\mathbf{n})] = f^2(l_n, m_n, s_n)Q_n. \quad (6)$$

The subscript *n*s on the cone contrasts are to indicate that this is the noise stimulus. In Equations 5 and 6, Q_t and Q_n are constants that are determined solely by the spatial and temporal aspects of the stimulus (see Appendix A for their values in the present study).

The main assumption of Giulianini and Eskew is "decision stage linearity" (2007, equation 1.3): that, at threshold, the relationship between the effect of an external noise within a detection mechanism is

$$E[Mech(\mathbf{v})] = N_0 + aE[Mech(\mathbf{n})] \quad (7)$$

with a a constant (see below). Inserting Equations 5 and 6 into Equation 7, we can express the S cone increment or decrement EvN as

$$f^2(0, 0, s_{nt})Q_t = N_0 + af^2(l_n, m_n, s_n)Q_n. \quad (8)$$

It is simple to show that this EvN is *approximately* linear for many smooth nonlinear cone combinations, including the best nonlinear model, $ks + \text{sign}(bl + dm)(bl + dm)$, of Giulianini and Eskew (2007), so the apparent linearity of our measured EvNs does not necessarily rule out nonlinear cone combination.

Note that if the cone combination is odd-symmetric, $f(\mathbf{v}) = -f(-\mathbf{v})$, as it is for a bipolar chromatic detection mechanism, then the mechanism noises produced by our noise stimuli are identical for the two test polarities, whether or not the mechanism is linear, because the response is squared in the energy computation.

If the chromatic mechanism is a linear combination of cone contrasts, then $f(\,)$ may be written as an inner product of a mechanism vector **f** (the vector of cone weights W_L, W_M, and W_S) and a vector representing the test **t** or noise **n** cone contrasts (*l, m, s*) and Equation 8 becomes

$$E_t = (\mathbf{f} \cdot \mathbf{t})^2 Q_t = N_0 + a(\mathbf{f} \cdot \mathbf{n})^2 Q_n. \quad (9)$$

Because the spatiotemporal characteristics of the test and noise were not varied in the present experiment, differences between S+ and S– could be attributed to differences in a (caused by spatiotemporal integration or contrast gain differences), **f** (overall and relative chromatic mechanism sensitivity), or both. The magnitudes reported in Table 2 are $\sqrt{a}|\mathbf{f}|$.